Micro-Scale Chemo-Mechanical Modeling of Li-Ion Batteries

ME5204 Finite Element Analysis (course project)

Ruthwik Chivukula

Department of Mechanical Engineering,
Indian Institute of Technology Madras, Chennai - 600036, India.
me21b166@smail.iitm.ac.in

Abstract

The need for efficient energy storage systems has demanded enormous efforts in increasing the longevity of Li-ion batteries, which are commonly subjected to severe particle level strains during production and cycling, impacting their lifetime. The study of these mechanical stresses that develop in the cells is quite complex involving multi-physics, requiring a highly coupled chemo-mechanical modeling. This review highlights the effect of intercalation induced mechanical stresses on concentration of Li-ion, using Finite Element Analysis. We compare the results obtained with the existing literature work in this field. In total, simulations of spherical active particles suggest that effective diffusion coefficient increases when stress dependencies are accounted in the formulation of concentration calculations, implying stress enhances diffusion.
Keywords: chemo-mechanical, diffusion, intercalation, lithiation

1 Introduction

The most common energy storage system is currently the Li-ion battery. This type of battery consists primarily of an anode, cathode, and a porous separator. The cathode (positive electrode) and the anode (negative electrode) are porous structures filled with additional electrolyte and binding agents to enhance the electrical conductivity and mechanical stability of the entire electrode. The anode and cathode contain active particles which are typically pockets that can accommodate and store charge. During lithiation/delithiation, the Li-ions diffuse and settle down in these active particles of the cathode/anode. The separator allows the transport of lithium ions between the anode and cathode during charging and discharging periods. Common cathodic materials include: Lithium Cobalt Oxide, Lithium Manganese Oxide, and Lithium Iron Phosphate. Each material is used for different applications depending on the need for specific battery life or discharge capacity. In this work, we will be assuming the cathodic material to be $LiMn_2O_4$ for all the future modeling and analysis. The anode is preferably made of graphite.

Li-intercalation induces mechanical stresses as the Li-ions now reside in the active particles of the cathode and anode, developing additional forces in the electrode system. These stresses can in turn effect the rate of diffusion of Li-ion, making it a two-way coupled multi-physics problem where both concentration of Li-ions and stresses in the electrode are interdependent. We use the stress-strain relations and diffusion equation to mathematically formulate the problem. Prussin

[1] previously treated concentration gradients in the stress-strain relations analogously to those generated by temperature gradients, which will be adopted even in the present work. The study of Li-ion cells can be done at different scales ranging from atomic scale to module scale. We will be interested particularly in the particle scale which is also considered as micro-scale modeling and our area of concern is determination of localized particle level stresses and concentrations in the cathode.

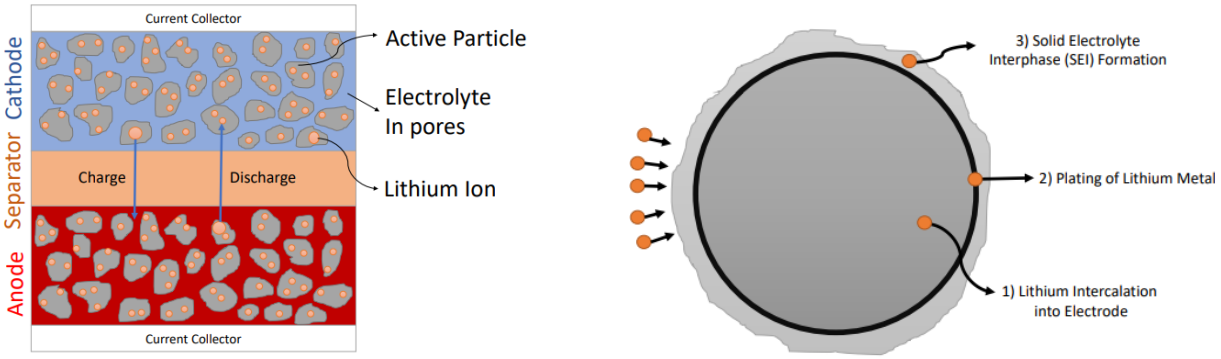

(a) Components of a Li-ion battery

(b) Reactions at the active particle level

Figure 1: Overview of Li-ion battery structure and reactions [2]

Parameter	Symbol and dimensions	Value
Young's modulus	E (GPa)	10
Poisson's ratio	ν	0.3
Partial molar volume	$\Omega(\mathrm{m}^3/\mathrm{mol})$	3.497×10^{-6}
Diffusion coefficient	$D(\mathrm{m}^2/\mathrm{s})$	7.08×10^{-15}

Table 1: Material properties of Mn_2O_4

2 Governing equations and weak form

2.1 Strong form

2.1.1 Stress-strain relations

Analogous to stress strain relations including thermal effects, the stress-strain relation with the existing of concentration gradients can be written as:-

$$\epsilon_{ij} = E\left[(1+\nu)\sigma_{ij} - \nu\sigma_{kk}\delta_{ij}\right] + \frac{\tilde{c}\Omega}{3}\delta_{ij} \tag{1}$$

Where $\tilde{c} = c - c_0$ is the concentration change of the diffusion species from the original value. Ω is the partial molar volume of solute, ν is the Poisson's ratio and E is the Young's modulus of the cathodic material. Equation 1 can be rewritten to obtain the expression for the components of stresses

$$\sigma_{ij} = 2\mu\epsilon_{ij} + (\lambda\epsilon_{kk} - \beta\tilde{c})\delta_{ij} \tag{2}$$

where $\mu = \frac{E}{2(1+\nu)}, \lambda = \frac{2\nu\mu}{(1-2\nu)}$, and $\beta = \frac{\Omega(3\lambda+2\mu)}{3}$. The relation between strain tensor and displacement $\mathbf{u}$ can be stated as:

$$\epsilon_{ij} = \frac{1}{2}\left(\frac{\partial u_i}{\partial x_j} + \frac{\partial u_j}{\partial x_i}\right) \tag{3}$$

The equilibrium condition, ignoring body forces is,

$$\nabla \cdot \boldsymbol{\sigma} = 0 \tag{4}$$

Combining Equation 2, 3 and 4 leads to the displacement equations

$$\mu\nabla^2 u_i + (\lambda+\mu)u_{k,ki} - \beta\tilde{c}_{,i} = 0 \quad (i = 1, 2, 3) \tag{5}$$

2.1.2 Diffusion equation

As we can see in Equation 1 and 2, intercalation stresses depend on the values of concentration profile. Concentration is obtained by modeling the lithiation process as a diffusion process. The chemical potential gradient is the driving force for the movement of lithium ions. The velocity of lithium ions can be expressed as

$$\mathbf{v} = -M\nabla\mu \tag{6}$$

where M is the mobility of lithium ions, and μ is the chemical potential. The chemical potential for an ideal solid solution can be given as

$$\mu = \mu_0 + RT\ln \mathrm{X} - M\Omega\sigma_h \tag{7}$$

Where μ_0 is a constant, R is the gas constant, T is absolute temperature, X is molar fraction of Li-ion, Ω is partial molar volume of Li-ion and σ_h is hydrostatic stress, given as $\frac{\sigma_{11}+\sigma_{22}+\sigma_{33}}{3}$. The species flux can then be written as

$$\mathbf{J} = -c\mathbf{v} = -Mc\nabla\mu \tag{8}$$

We assume there is no temperature gradient inside the particle. Under this assumption, substituting Equation 7 in 8 and simplifying it further, we obtain

$$\mathbf{J} = -D\left(\nabla c - \frac{\Omega c}{RT}\nabla\sigma_h\right) \tag{9}$$

where $D = MRT$ is diffusion coefficient. Invoking the mass conservation principle over the concentration of Li-ions in the particle gives

$$\frac{\partial c}{\partial t} + \nabla \cdot \mathbf{J} = 0 \tag{10}$$

Then, substituting 9 in 10 finally results

$$\frac{\partial c}{\partial t} = D\left(\nabla^2 c - \frac{\Omega}{RT}\nabla c \cdot \nabla\sigma_h - \frac{\Omega c}{RT}\nabla^2\sigma_h\right) \tag{11}$$

2.1.3 Computational domain

The Active particles are modeled as spherical bodies under the assumption of symmetric behavior with respect to θ and ϕ. Hence the computational domain reduces from 3-D to 1-D, the only variable being, the radial distance, r. We now compute the above obtained strong form results in terms of the radial coordinates before proceeding to the weak form formulation.

The equilibrium equation 4 in this case, simplifies to

$$\frac{\partial \sigma_r}{\partial r} + \frac{2}{r}(\sigma_r - \sigma_t) = 0 \tag{12}$$

and the stress-strain relations (refer 1) are

$$\epsilon_r = \frac{1}{E}(\sigma_r - 2\nu\sigma_t) + \frac{\Omega}{3}\tilde{c} \tag{13}$$

$$\epsilon_t = \frac{1}{E}\left[\sigma_t - \nu(\sigma_t + \sigma_r)\right] + \frac{\Omega}{3}\tilde{c} \tag{14}$$

strain-displacement relations (refer 3) boil down to

$$\epsilon_r = \frac{\partial u}{\partial r} \tag{15}$$

$$\epsilon_t = \frac{u}{r} \tag{16}$$

Substituting these relations into Equation 5, we finally obtain the governing differential equation for displacement as

$$\frac{\partial^2 u}{\partial r^2} + \frac{2}{r}\frac{\partial u}{\partial r} - \frac{2u}{r^2} = \frac{1+\nu}{1-\nu}\frac{\Omega}{3}\frac{\partial \tilde{c}}{\partial r} \tag{17}$$

Observe that the displacement equation depends upon concentration. Given the concentration, one can analytically solve for u using Bessel functions.

Similarly, expressing the concentration conservation equation 11 in terms of radial coordinates yields the following differential equation

$$\frac{\partial c}{\partial t} = D\left[\frac{\partial^2 c}{\partial r^2} + \frac{2}{r}\frac{\partial c}{\partial r} - \frac{\Omega}{RT}\frac{\partial c}{\partial r}\frac{\partial \sigma_h}{\partial r} - \frac{\Omega c}{RT}\left(\frac{\partial^2 \sigma_h}{\partial r^2} + \frac{2}{r}\frac{\partial \sigma_h}{\partial r}\right)\right] \tag{18}$$

The hydrostatic stress given as $\sigma_h = \frac{\sigma_r + 2\sigma_t}{3}$ can be computed in terms of $\tilde{c}$ using equation 17 which can be substituted back into equation 18 to obtain the following

$$\frac{\partial c}{\partial t} = D\left[\frac{\partial^2 c}{\partial r^2} + \frac{2}{r}\frac{\partial c}{\partial r} + \alpha\left(\frac{\partial c}{\partial r}\right)^2 + \alpha c\left(\frac{\partial^2 c}{\partial r^2} + \frac{2}{r}\frac{\partial c}{\partial r}\right)\right] \tag{19}$$

where $\alpha = \frac{\Omega}{RT}\left[\frac{(2\Omega E)}{9(1-\nu)}\right]$. The equation 19 is decoupled, containing only concentration terms. However it is a non-linear equation and should be handled appropriately using techniques like Picard iteration. Our objective hereon is to solve this equation and find the concentration profile. Once the concentration profile is found, it can be re-substituted back in equation 17 to obtain the displacement field $\mathbf{u}$ and eventually σ_r and σ_t.

2.2 Weak form

Using finite elements we aim to solve the non-linear equation 19. Invoking Galerkin orthogonality and Gauss divergence we shall arrive at the weak form.

The weak form of the governing equation in spherical coordinates is expressed as:

$$\begin{aligned}
&\int_0^{2\pi}\int_0^{\pi}\int_0^{r_0} w\frac{\partial c}{\partial t}r^2\sin\theta\,dr\,d\theta\,d\phi \\
&= \int_0^{2\pi}\int_0^{\pi}\int_0^{r_0} Dw\frac{\partial^2 c}{\partial r^2}r^2\sin\theta\,dr\,d\theta\,d\phi \\
&+ \int_0^{2\pi}\int_0^{\pi}\int_0^{r_0} Dw\frac{2}{r}\frac{\partial c}{\partial r}r^2\sin\theta\,dr\,d\theta\,d\phi \\
&+ \int_0^{2\pi}\int_0^{\pi}\int_0^{r_0} Dw\alpha\left(\frac{\partial c}{\partial r}\right)^2 r^2\sin\theta\,dr\,d\theta\,d\phi \\
&+ \int_0^{2\pi}\int_0^{\pi}\int_0^{r_0} Dw\alpha c\left(\frac{\partial^2 c}{\partial r^2}+\frac{2}{r}\frac{\partial c}{\partial r}\right)r^2\sin\theta\,dr\,d\theta\,d\phi
\end{aligned}$$

Where w is an arbitrary test function. Since the concentration is invariant of θ and ϕ, the weak form can be simplified as

$$4\pi\int_0^{r_0}\left[\underbrace{-w\frac{\partial c}{\partial t}r^2}_{(A)}+\underbrace{Dw\frac{\partial^2 c}{\partial r^2}r^2}_{(B)}+\underbrace{Dw\frac{2}{r}\frac{\partial c}{\partial r}r^2}_{(C)}+\underbrace{Dw\alpha\left(\frac{\partial c}{\partial r}\right)^2 r^2}_{(D)}+\underbrace{Dw\alpha c\frac{\partial^2 c}{\partial r^2}r^2}_{(E)}+\underbrace{Dw\alpha c\frac{2}{r}\frac{\partial c}{\partial r}r^2}_{(F)}\right]dr=0 \tag{20}$$

Let us evaluate the terms (B) and (E) individually by applying Gauss divergence.
(B):-

$$\int_0^{r_0} Dw\frac{\partial^2 c}{\partial r^2}r^2dr=\left[Dwr^2\frac{\partial c}{\partial r}\right]_{\partial\Omega}-\int_0^{r_0} Dr^2\frac{\partial w}{\partial r}\frac{\partial c}{\partial r}dr-\int_0^{r_0}2Dwr\frac{\partial c}{\partial r}dr$$

(E):-

$$\int_0^{r_0} Dw\alpha c\frac{\partial^2 c}{\partial r^2}r^2dr=\left[Dw\alpha r^2 c\frac{\partial c}{\partial r}\right]_{\partial\Omega}-\int_0^{r_0} D\alpha cr^2\frac{\partial w}{\partial r}\frac{\partial c}{\partial r}dr-\int_0^{r_0}2Dw\alpha rc\frac{\partial c}{\partial r}dr-\int_0^{r_0} Dw\alpha r^2\left(\frac{\partial c}{\partial r}\right)^2 dr$$

Substituting these results back into equation 20 gives us the final weak form

$$\int_0^{r_0}\left[\underbrace{w\frac{\partial c}{\partial t}r^2}_{\text{mass term}}+\underbrace{Dr^2\frac{\partial w}{\partial r}\frac{\partial c}{\partial r}}_{\text{bi-linear term}}+\underbrace{D\alpha cr^2\frac{\partial w}{\partial r}\frac{\partial c}{\partial r}}_{\text{non-linear term}}\right]dr=\underbrace{Dwr^2\left[(1+\alpha c)\frac{\partial c}{\partial r}\right]_{\partial\Omega}}_{\text{boundary term}} \tag{21}$$

2.3 Boundary conditions

We have to impose boundary conditions on both the governing equations, one for the stress or displacement equation and other for the concentration diffusion equation. As we are concerned only about the decoupled non-linear concentration equation, let us focus on the boundary conditions for

it. We apply a Neumann boundary condition which is given as

$$(1+\alpha c)D\frac{\partial c}{\partial r}\bigg|_{r=r_0} = \frac{i_n}{F} \tag{22}$$

Where i_n is the incident current density which we assume to be 2 $\frac{A}{\mathrm{m}^2}$ and F is the Faraday constant. r_0, radius of the active particle, for our problem setup is assumed to be 5×10^{-6} m. For the stresses, we set radial stress at the surface, $\sigma_r\Big|_{r=r_0} = 0$.

3 Discretization approach

As the problem statement is reduced from a 3-D spherical volume setup to a 1-D radial distance setup, we can adopt the 1-D hat functions Φ_I which are given by:

$$\phi_I(r) = \begin{cases} \frac{r-r_{I-1}}{r_I-r_{I-1}} & \text{for } r\in(r_{I-1},r_I) \\ \frac{r_{I+1}-r}{r_{I+1}-r_I} & \text{for } r\in(r_I,r_{I+1}) \\ 0 & \text{otherwise} \end{cases}$$

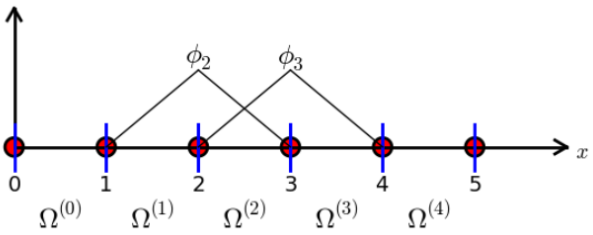

Figure 2: 1-D linear hat functions

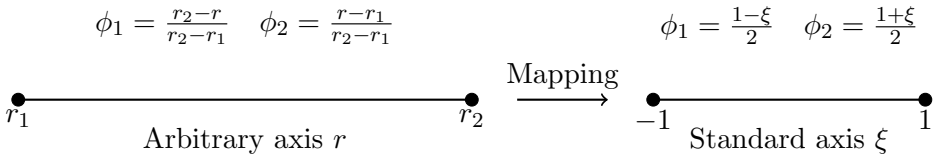

Number of points	Coordinates (ξ)	Weights
2	$-\frac{1}{\sqrt{3}}, \frac{1}{\sqrt{3}}$	1, 1
3	$0, \frac{\sqrt{3}}{5}, -\frac{\sqrt{3}}{5}$	$\frac{8}{9}, \frac{5}{9}, \frac{5}{9}$

The Gauss Quadrature points for 1-D problem are given above. We will be using two Gauss points for the numerical integration. The problem at hand is a temporal non-linear problem. We adopt an implicit temporal scheme for time marching as it is more stable and gives us the flexibility to choose larger time strides. The non-linearity in the weak form is handled by implementing Picard iteration. Therefore, we iterate over time-steps and for every time-step we perform the Picard iteration until the convergence criteria is met. The convergence criteria is

$$\|\text{new\_pred} - \text{old\_pred}\|_2 \leq \text{tolerance}$$

For the matrix formulation of each of the terms, we express the test function and the concentration as linear combination of hat functions.

$$c(r,t) = \sum_J \Phi_J c_J(t)$$
$$w(r,t) = \sum_I \Phi_I w_I(t)$$

we perform an element-wise thinking to formulate the local matrices. For an element,
mass term:-

$$\int_1^2 w\frac{\partial c}{\partial t}r^2 = \int_1^2 w\frac{(c^{t+1}-c^t)}{\Delta t}r^2 dr = \begin{bmatrix} w_1 & w_2 \end{bmatrix} \Big(\int_1^2 \begin{bmatrix} \phi_1 \\ \phi_2 \end{bmatrix} \begin{bmatrix} \phi_1 & \phi_2 \end{bmatrix} \frac{r^2}{\Delta t}\, dr \begin{bmatrix} c_1 \\ c_2 \end{bmatrix}^{t+1} - \int_1^2 \begin{bmatrix} \phi_1 \\ \phi_2 \end{bmatrix} \begin{bmatrix} \phi_1 & \phi_2 \end{bmatrix} \frac{r^2}{\Delta t}\, dr \begin{bmatrix} c_1 \\ c_2 \end{bmatrix}^{t} \Big)$$

bi-linear term:-

$$\int_1^2 Dr^2 \frac{\partial w}{\partial r}\frac{\partial c}{\partial r} = \begin{bmatrix} w_1 & w_2 \end{bmatrix} \int_1^2 \begin{bmatrix} \frac{\partial \phi_1}{\partial r} \\ \frac{\partial \phi_2}{\partial r} \end{bmatrix} \begin{bmatrix} \frac{\partial \phi_1}{\partial r} & \frac{\partial \phi_2}{\partial r} \end{bmatrix} Dr^2\, dr \begin{bmatrix} c_1 \\ c_2 \end{bmatrix}^{t+1}$$

non-linear term:-

$$\int_1^2 D\alpha c r^2 \frac{\partial w}{\partial r}\frac{\partial c}{\partial r} = \begin{bmatrix} w_1 & w_2 \end{bmatrix} \int_1^2 \begin{bmatrix} \frac{\partial \phi_1}{\partial r} \\ \frac{\partial \phi_2}{\partial r} \end{bmatrix} \begin{bmatrix} \frac{\partial \phi_1}{\partial r} & \frac{\partial \phi_2}{\partial r} \end{bmatrix} Dc^* r^2\, dr \begin{bmatrix} c_1 \\ c_2 \end{bmatrix}^{t+1}$$

c^* is initially guessed and iteratively corrected using Picard iteration until convergence,

$$\|\mathbf{c}^{t+1} - \mathbf{c}^*\|_2 \leq \text{tolerance}$$

boundary term:-

$$\begin{bmatrix} w_1 & w_2 \end{bmatrix} \begin{bmatrix} -Dr^2(1+\alpha c)\frac{\partial c}{\partial r}\Big|_1 \\ Dr^2(1+\alpha c)\frac{\partial c}{\partial r}\Big|_2 \end{bmatrix}$$

These local matrices are appropriately assembled to form global matrices of dimension $N_{\text{nodes}} \times N_{\text{nodes}}$. The boundary term will be a vector of dimension $N_{\text{nodes}} \times 1$. The intermediate entries of the boundary term cancel out as they form action reaction pairs leaving only the initial and final entries as non-zero. The first entry is also zero here as r = 0. The last entry will be $r_o^2 \frac{i_n}{F}$. Hence, the assembled global boundary vector is

$$\mathbf{BC} = \begin{bmatrix} 0 \\ 0 \\ \vdots \\ 0 \\ \frac{r_0^2 i_n}{F} \end{bmatrix}$$

The final equation looks as

$$M\mathbf{C}^{t+1} + D\Delta t \left(K\mathbf{C}^{t+1} + K'\mathbf{C}^{t+1}\right) = \Delta t\, \mathbf{BC} + M\mathbf{C}^t$$

where M is the assembled global mass matrix, K is the assembled global bi-linear matrix, K' is the assembled global non-linear matrix and $\mathbf{BC}$ is the assembled global boundary vector.

4 Numerical Example

Our objective is to find the concentration profile as a function of r, the radial distance from the center. We will be analyzing two variants here, one in which the concentration formulation accounts for mechanical stresses and other in which the concentration formulation doesn't account for mechanical stresses. The former case is what we have formulated in the above section. In the latter case, the only difference being, the non-linear term will not appear in the problem formulation. We aim to compare both these concentration profiles and draw insights about their behavior.

As the finite element formulation is done, we have to choose the optimum number of nodes and the optimal time stride for our problem. This is done via mesh convergence plots and time convergence plots.

We will be performing the mesh convergence test and time convergence test individually for concentration formulation with stress and without stress.

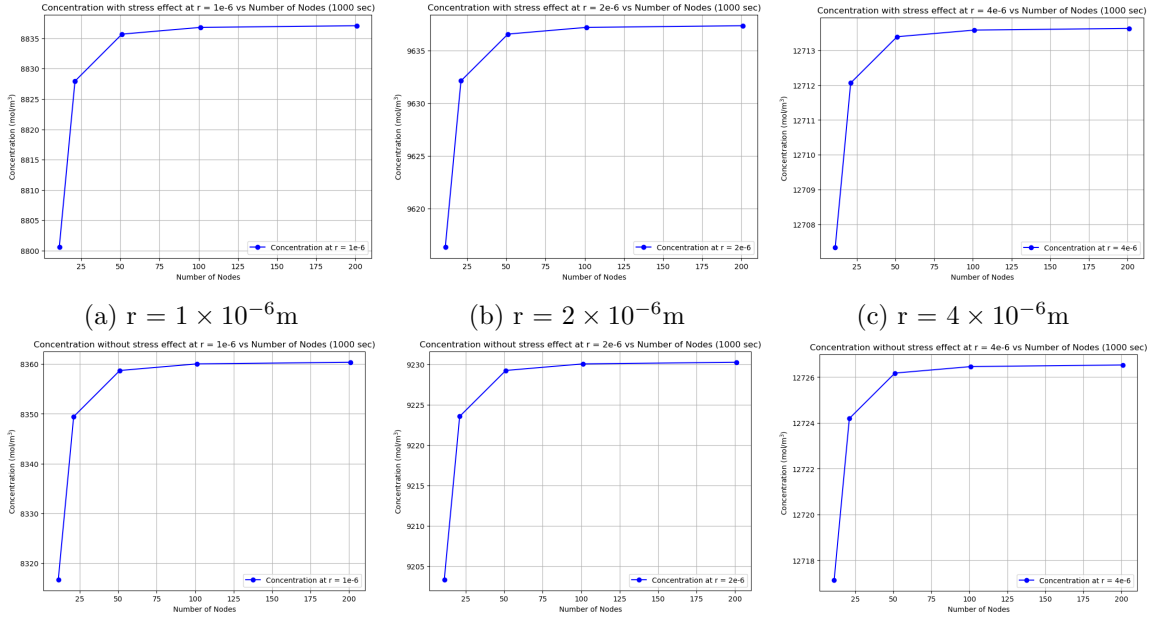

(a) r = 1×10^{-6}m (b) r = 2×10^{-6}m (c) r = 4×10^{-6}m

(d) r = 1×10^{-6}m (e) r = 2×10^{-6}m (f) r = 4×10^{-6}m

Figure 3: Mesh convergence at three points for concentration with stress effects (top row) and without stress effects (bottom row) (Δt = 10 sec)

no. of nodes	**mesh size** (μm)	**error % with stress**	**error % without stress**
11	0.1	-	-
21	0.05	0.31	0.39
51	0.02	0.087	0.11
101	0.01	0.012	0.015
201	0.005	0.003	0.004

Table 2: Relative error in concentration for varying number of nodes(r = 1e-6 m)

It is noticeable that the relative error decreases as the mesh gets finer. This validates our mesh convergence test. Similarly, it can be observed, the relative error decreases as the time-step

Δt (sec)	error % with stress	error % without stress
100	-	-
10	0.36	0.48
1	0.02	0.03
0.1	0.002	0.003

Table 3: Relative error in concentration for varying time step sizes(r = 1e-6 m)

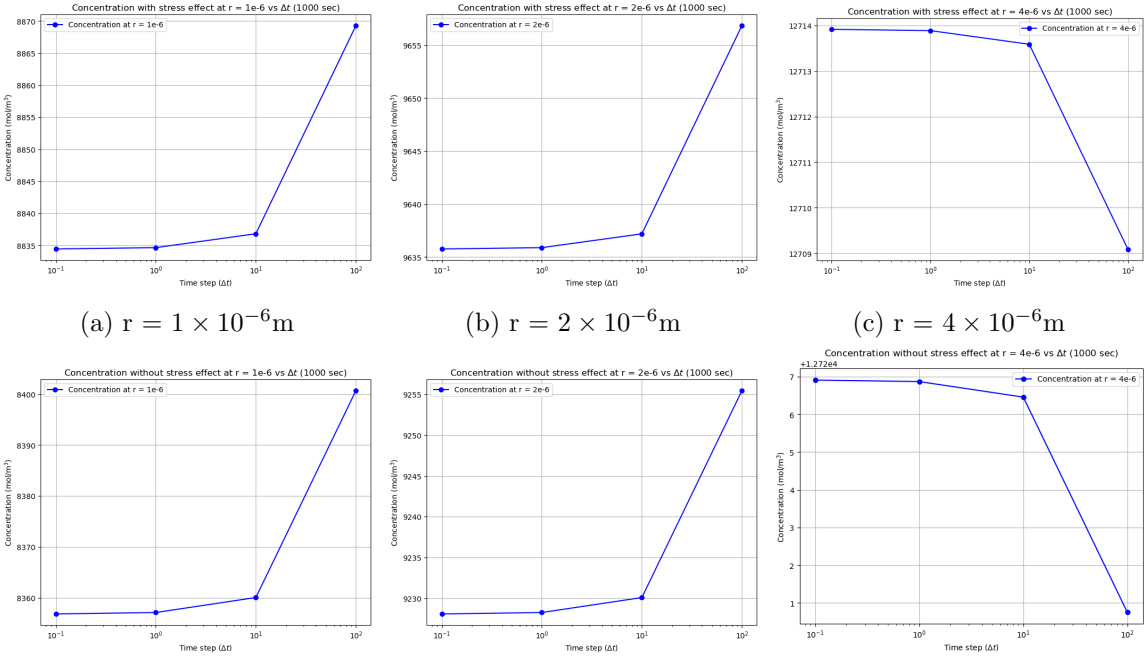

(a) r = 1×10^{-6}m (b) r = 2×10^{-6}m (c) r = 4×10^{-6}m

(d) r = 10^{-6}m (e) r = 2×10^{-6}m (f) r = 4×10^{-6}m

Figure 4: Time convergence at three points for concentration with stress effects (top row) and without stress effects (bottom row) (nodes = 101)

decreases, confirming the temporal convergence test. Based on these convergence results (refer figure 3, 4), we can choose number of nodes = 101 and Δ t = 1 second.

Using these values, we obtain the concentration profile as a function of radial distance. We compare the results obtained against one of the reference literature work [3] (refer figure 5). The results match almost perfectly with the reference material implying the finite element formulation is accurate. We also plot the concentration profile for a given cross-section of the spherical active particle to visualize the concentration gradient (refer figure 6).

5 Conclusions

Observing the figure 5 carefully, we can infer that the gradient of concentration profile with stress effects is smaller in comparison to concentration profile without stress effects. This observation can also be drawn from the 2-D heat map (refer figure 6). The concentration cloud is diffused in the former case while it looks denser in the latter. These results align with the theoretical results as

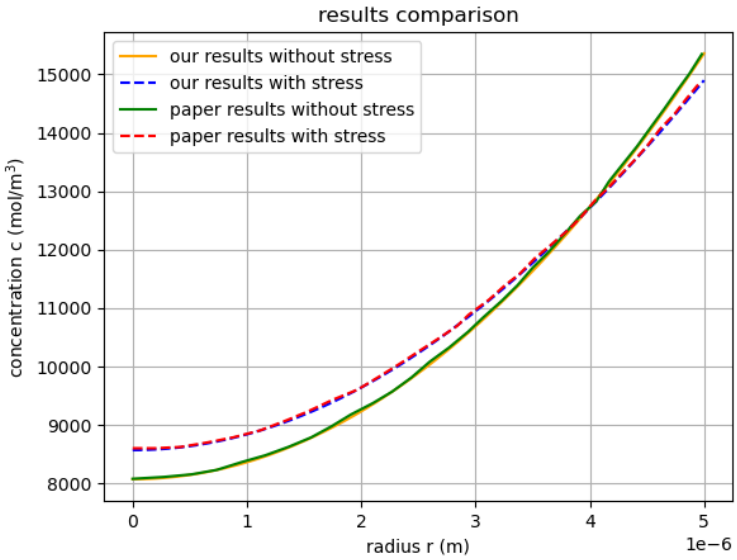

Figure 5: results comparison for t = 1000 sec

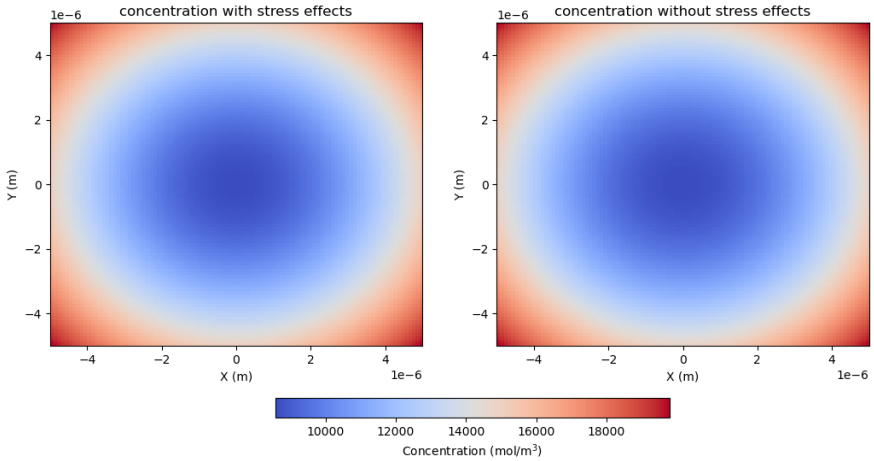

Figure 6: concentration profile of a 2-D cross section of the spherical particle with and without stress effect

well. Theoretically, the species flux is given by

$$\mathbf{J} = -D(1 + c\alpha)\frac{\partial c}{\partial r}$$

So, the effective diffusion coefficient increases from D to $D(1 + c\alpha)$ where $c\alpha$ is a positive constant. As the diffusion coefficient increased, the concentration is distributed across the domain and hence the ion-cloud is less dense. This can be interpreted even intuitively. When the stresses developed are not oblivious of the ion-concentration in the particle, the particle tends to push away the ions, reducing the local concentration which in turn reduces local stresses, enabling the particle to be at a stable, lower energy state. In conclusion, we can state that stress enhances diffusion.

6 Learning Outcomes and Acknowledgment

The present project has taught me how to deal with two-way coupled equations. Studying the chemo-mechanical governing equations and formulating the weak form for a complex setup has further strengthened my understanding of the underlying concepts. The non-linear temporal differential equation gave me an opportunity to implement Picard iteration appropriately along with time marching. The physics of the problem as observed from the numerical aspect perfectly aligns with the theoretical view point, backing the FE code formulation. The interdependency between stress and concentration is more clearly realized now as compared to the beginning of the project. I am obliged and grateful to Prof. Sundar for assigning this exploratory project and patiently clarifying all queries throughout the course project.

7 References

References

[1] S. Prussin. Generation and distribution of dislocations by solute diffusion. *Journal of Applied Physics*, 32(10):1876–1881, 1961.

[2] Miklos Johann Zoller. *Micro Scale Lithium Ion Battery Modeling with the Finite Element Method*. PhD thesis, University of California, Berkeley, 2020. Peer-reviewed, Thesis/Dissertation.

[3] Xiangchun Zhang et al. Numerical simulation of intercalation-induced stress in li-ion battery electrode particles. *J. Electrochem. Soc.*, 154:A910, 2007.